PHYSICAL REVIEW B VOLUME 57, NUMBER 9 1 MARCH 1998-I

Martensite-austenite transition and phonon dispersion curves of $Fe_{1-x}Ni_x$ studied by molecular-dynamics simulations

R. Meyer* and P. Entel†

Theoretische Tieftemperaturphysik, Gerhard-Mercator-Universität, Gesamthochschule Duisburg,
Lotharstraße 1, 47048 Duisburg, Germany

(Received 16 April 1997; revised manuscript received 30 September 1997)

We have done molecular-dynamics simulations of $Fe_{1-x}Ni_x$ employing a semiempirical model. We present a phase diagram of the martensite-austenite transition temperatures as a function of the Ni concentration which is in good agreement with experimental observations. In addition to this we have calculated the phonon dispersion curves of Fe and Ni from the model. Results show that the vibrational properties of the metals are well reproduced by the embedded-atom-method potentials. Finally, we have derived the phonon dispersion relations of bcc $Fe_{80}Ni_{20}$. We find rather low energies of the [110]-TA_1 phonons with a strong temperature dependence which we attribute to instabilities of Ni in the bcc phase. We do not find any indications of a soft mode at the martensite-austenite transition in $Fe_{1-x}Ni_x$. [S0163-1829(98)01206-5]

I. INTRODUCTION

Although martensitic transformations have been studied for more than a century, the atomistic processes leading to the structural transition are still a subject of debate. While most studies of martensitic phenomena concentrate on the austenite to martensite transition, only little effort has been put into investigations of the reverse transformation. This is particularly true in the case of $Fe_{1-x}Ni_x$ alloys exhibiting a martensitic transformation from fcc austenite to bcc martensite with decreasing temperature (see, for instance, Ref. 1). For these alloys only few data in the martensitic phase exist since there are big difficulties in the preparation of single crystals with bcc structure. Under such circumstances molecular-dynamics simulation can be a powerful tool which allows us to study the properties of the martensitic phase even beyond its stability boundaries. But, in order to obtain physically relevant results, great care has to be taken in choosing the model used for the description of the system in the simulations.

In this work we present results of molecular-dynamics simulations of $Fe_{1-x}Ni_x$ alloys employing a recently developed semiempirical model.[2,3] Although bcc $Fe_{1-x}Ni_x$ alloys show ferromagnetic order at low temperatures, this model does not consider magnetism in an explicit way, but rather only through the fitting of the potentials to some low-temperature properties of the metals Fe and Ni. Despite this shortcoming the model reveals a transformation from a bcc structure to a closed-packed structure with increasing temperature. We have studied the concentration dependence of the transition temperatures and the orientational relationships of this transition with molecular-dynamics simulations. In order to see whether the model used in our simulations gives a reasonable description of the vibrational properties of the pure metals, we have calculated the phonon spectra of Fe and Ni resulting from the potentials by diagonalization of the dynamical matrix. Finally we have derived phonon spectra of $Fe_{80}Ni_{20}$ from molecular-dynamics simulations by calculation of the velocity autocorrelation function and the dynamical structure factor. We present the phonon energies at room temperature along five high-symmetry lines. Special attention has been paid to the dispersion of the [110]-TA_1 modes which we have calculated at several temperatures beyond the austenite transition temperature. The results show a strongly temperature-dependent softening of the [110]-TA_1 phonons well below the martensite-austenite transition temperature. This behavior is similar to experimental findings in the martensitic transformation of some nonferrous alloys.[4,5] In order to understand these effects we have calculated the spectrum of pure bcc Ni and Fe, using the lattice constant of $Fe_{80}Ni_{20}$ we obtained in our simulations. From the resulting spectrum of bcc Ni it can be seen that there is a general tendency of Ni to destabilize the bcc structure.

II. DETAILS OF THE COMPUTATIONS

A. EAM potentials

In our molecular-dynamics simulations we have employed a model which has recently been constructed for the simulation of the austenite transition in $Fe_{1-x}Ni_x$ alloys.[2,3] This model relies on the embedded-atom method (EAM), introduced by Daw and Baskes,[6] which allows for a better description of the elastic properties of metals and alloys than ordinary pair potentials do. For details concerning the EAM we refer to Refs. 6, 7. The potential energy E of the system is written as

$$E=\sum_i \mathcal{F}_i(\rho_i)+\sum_{i\neq j}\frac{Z_i(r_{ij})Z_j(r_{ij})}{r_{ij}}, \tag{1}$$

where the summations run over all atoms and r_{ij} is the distance between the atoms i and j. The embedding charge density ρ_i at the position of atom i is approximated by a superposition of element-dependent contributions $\rho_j^{\mathrm{at}}=\rho_{Fe}^{\mathrm{at}},\rho_{Ni}^{\mathrm{at}}$ of the surrounding j atoms

$$\rho_i=\sum_{j\neq i}\rho_j^{\mathrm{at}}(r_{ij}). \tag{2}$$

0163-1829/98/57(9)/5140(8)/$15.00

TABLE I. Parameters used for the calculation of the embedding charge densities.

	N_v	N_{4s}	R_c (a.u.)
Fe	8	0.57	8.332
Ni	10	0.85	8.777

Like Daw and Baskes[6] we use the appropriate double-ζ wave functions Ψ of Clementi and Roetti[8] for the calculation of the atomic contributions

$$\rho^{\mathrm{at}}(r)=N_{4s}|\Psi_{4s}(r)|^2+(N_v-N_{4s})|\Psi_{3d}(r)|^2-\rho_c. \quad (3)$$

Here N_v and N_{4s} are the numbers of valence and s symmetry electrons. In order to get a finite interaction range, $\rho^{\mathrm{at}}(r)$ is truncated at a cutoff radius R_c between the third- and fourth-nearest-neighbor shells and the constant shift ρ_c is applied to obtain a continuous behavior of the embedding charge density at $r=R_c$. The values of N_v, N_{4s}, and R_c used for Fe and Ni in this work are summarized in Table I.

The first term in Eq. (1) is a sum of the embedding energies of the atoms, while the second term represents a pair-potential adopting a screened Coulomb interaction. The embedding functions $\mathcal{F}_i=\mathcal{F}_{\mathrm{Fe}},\mathcal{F}_{\mathrm{Ni}}$ and the effective charges $Z_i=Z_{\mathrm{Fe}},Z_{\mathrm{Ni}}$ are cubic spline functions. The parameters of these functions have been determined by a fit to experimental data of the lattice constants a_0, sublimation energies E_s, elastic constants C_{11}, C_{12}, and C_{44}, vacancy formation energies E_v, and some selected phonon frequencies of pure Fe and Ni. The parameters of the potential are summarized in Tables II and III. In Table IV we compare the experimental data used for the fit and the theoretical values, calculated from the EAM potentials. Additionally the energy differences between the bcc and the fcc structure of the metals are reported.

B. Molecular-dynamics simulations

With the model described in the preceeding section we performed standard molecular-dynamics simulations[15] employing the Verlet algorithm with a time step of 1.5 fs and periodic boundary conditions in all of our calculations. In order to determine the transformation temperatures we have performed a series of simulations starting with initial configurations of 1024 atoms, arranged on an ideal lattice of $8\times8\times8$ cubic bcc cells. The concentration of the randomly distributed Ni atoms varied in the range $0\%<x<40\%$. With these configurations, simulations were done in the NTP ensemble generated by the Nosé-Hoover thermostat method[16,17] combined with the Parrinello-Rahman scheme.[18] The latter method had to be used in order to be able to simulate a structural phase transition with a volume change. Starting about 300–500 K below the transition temperatures the temperature was increased in steps of 100 K well below the (estimated) transition temperatures and in steps of 25 K near the transition. At each temperature 5000 simulation steps (7.5 ps) were performed until the structural transition occurred. At the structural transition deviations from the cu-

TABLE II. Parameters determining the embedding functions $\mathcal{F}_{\mathrm{Fe}}$ and $\mathcal{F}_{\mathrm{Ni}}$. Energies are in units of Ry. The embedding densities are given in terms of the equilibrium densities $\rho_0=2.776\times10^{-3}$ a.u. and 4.187×10^{-3} a.u. for Fe and Ni, respectively.

ρ/ρ_0	$\mathcal{F}_{\mathrm{Fe}}$	$\mathcal{F}''_{\mathrm{Fe}}$	$\mathcal{F}_{\mathrm{Ni}}$	$\mathcal{F}''_{\mathrm{Ni}}$
0.0	0.0	0.0	0.0	0.0
0.5	−0.2823		−0.2695	
1.0	−0.4276		−0.3961	
2.0	−0.3030		−0.2654	
2.3	0.0	0.0	0.0	0.0

TABLE III. Parameters determining the effective charge functions Z_{Fe} and Z_{Ni}. Charges are given in units of e^-, distances in units of the appropriate equilibrium lattice constants $a_0=5.42$ a.u. and 6.65 a.u. for Fe and Ni, respectively.

r/a_{Fe}	Z_{Fe}	Z'_{Fe}	r/a_{Ni}	Z_{Ni}	Z'_{Ni}
0.0	26.0	0.0	0.0	28.0	0.0
0.70	1.4403		0.60	0.9874	
0.87	0.2452		0.71	0.1596	
0.94	0.1491		0.85	0.0	0.0
1.00	0.0734				
1.20	0.0	0.0			

TABLE IV. Experimental data and the corresponding calculated values used in the fit of the parameters of the potential. Phonon frequencies are given in THz.

	Fe		Ni	
	Expt.	Calc.	Expt.	Calc.
a_0 (a.u.)	5.42	5.42	6.65	6.65
E_s (Ry)	0.315	0.315	0.327	0.327
E_v (Ry)	0.110	0.109	0.110	0.109
$E_{\mathrm{bcc}}-E_{\mathrm{fcc}}$ (mRy)	−3.66[a]	−2.79	4.41[b]	3.39
C_{11} (10^{12} dyn/cm^2)	2.431[c]	2.510	2.612[d]	2.279
C_{12} (10^{12} dyn/cm^2)	1.381[c]	1.304	1.508[d]	1.563
C_{44} (10^{12} dyn/cm^2)	1.219[c]	1.187	1.317[d]	1.111
$\mathbf{q}=0.685\,\frac{2\pi}{a_0}[111]$	5.73[e]	5.12		
	8.08[e]	8.63		
$\mathbf{q}=\frac{2\pi}{a_0}[\frac{1}{2}\frac{1}{2}\frac{1}{2}]$			8.88[f]	9.04
			4.24[f]	4.06
$\mathbf{q}=\frac{2\pi}{a_0}[1\,0\,0]$	8.56[e]	8.46	8.55[f]	9.15
			6.27[f]	6.29
$\mathbf{q}=\frac{2\pi}{a_0}[\frac{1}{2}\frac{1}{2}0]$	9.26[e]	9.93	7.63[f]	7.81
	6.46[e]	6.03	6.15[f]	6.44
	4.47[e]	4.27	4.36[f]	4.06

[a] Reference 9.
[b] Reference 10.
[c] Reference 11.
[d] Reference 12.
[e] Reference 13.
[f] Reference 14.

bic shape of the simulation box occurred which allowed the detection of the phase transition. Additionally the structure of the system was monitored through calculation of the radial distribution function[15] which also reflects the phase transition.[2] Another system of this size with a Nickel concentration $x=20\%$ (205 atoms) has been simulated over a complete temperature cycle between 0 and 1000 K in steps of 25 K.

The phonon-dispersion curves were derived from simulations with one configuration of 12×12×12 bcc cells (3456 atoms) containing a Ni concentration $x=20\%$ (691 atoms). The martensite-austenite transition temperature of this configuration is 750 K. Since the Parrinello-Rahman scheme and the Nosé-Hoover thermostat change the trajectories of the atoms, the phonon-dispersion curves had to be derived from simulations with fixed simulation cell and constant energy (NVE ensemble). This required the determination of the zero-pressure lattice parameters of the configuration. Below the austenite transition temperature these could be obtained from simulations with the Parrinello-Rahman scheme. Above the austenite transition temperature we used lattice parameters extrapolated from the low-temperature data. By doing so we were able to investigate the vibrational properties of the alloy in the martensite phase even beyond its stability boundary, since the fixed simulation cell suppresses the structural phase transition. At each temperature 40 000 simulation steps (60 ps) were done, using the atomic positions of every tenth step to calculate the dynamical structure factor

$$S(\mathbf{q},\omega)=\frac{1}{N}\int\frac{dt}{2\pi}e^{i\omega t}\sum_{i,j}\langle e^{i\mathbf{q}\cdot\mathbf{R}_i(0)}e^{-i\mathbf{q}\cdot\mathbf{R}_j(t)}\rangle, \tag{4}$$

which is closely related to the cross section measured in neutron-diffraction experiments.[19] Here N is the number of particles and $\mathbf{R}_i$ is the position of atom i at time t. While in the case of a nearly harmonic system $S(\mathbf{q},\omega)$ shows sharp peaks at the phonon frequencies, anharmonic effects lead to finite phonon lifetimes which broaden the peaks of the dynamical structure factor and shift them to lower frequencies. For a harmonic oscillator which is damped by a stochastic friction, the dynamical structure factor can be shown to be[20]

$$S(\omega)=\frac{\hbar}{\pi M_0}\left[\frac{1}{1-e^{-\hbar\omega/k_BT}}\right]\frac{\Gamma\omega}{(\omega^2-\omega_0^2)^2+(\Gamma\omega)^2}, \tag{5}$$

where M_0 is the particle mass, ω_0 is the frequency of the undamped oscillator and Γ is the friction constant. In the classical limit $\hbar\rightarrow 0$ this result is reduced to

$$S(\omega)=\frac{1}{\pi M k_BT}\frac{\Gamma}{(\omega^2-\omega_0^2)^2+(\gamma\omega)^2}. \tag{6}$$

It has been pointed out by Zhang *et al.*[21] that the dynamical structure factor can show an anomalous Brillouin-zone behavior. This is especially important if transversal phonon modes are considered since in this case one has to choose $\mathbf{q}$ vectors apart from the first Brillouin zone.[22] These problems can be avoided if the phonon frequencies are derived from the velocity autocorrelation function[23]

$$g_{\alpha\alpha}(\mathbf{q},\omega)=\int_{-\infty}^{\infty}dt\sum_n e^{i\omega t}e^{i\mathbf{q}\cdot\mathbf{R}_n^0}\left[\frac{\langle v_n^\alpha(t)v_0^\alpha(0)\rangle}{\langle v_n^\alpha(0)v_0^\alpha(0)\rangle}\right], \tag{7}$$

with

$$\langle v_n^\alpha(t)v_0^\alpha(0)\rangle=\frac{1}{MN}\sum_\tau\sum_j v_{n+j}^\alpha(t+\tau)v_n^\alpha(\tau). \tag{8}$$

Here M is the number of time steps used for the calculation, $\mathbf{R}_n^0$ is the ideal lattice position of particle n, and $v_n^\alpha(t)$ is the α component of the velocity of particle n at time t. It can be seen from the definition in Eq. (7) that the velocity autocorrelation function $g_{\alpha\alpha}(\mathbf{q},\omega)$ does not show an anomalous zone behavior. In case of a purely harmonic system $g_{\alpha\alpha}(\mathbf{q},\omega)$ is proportional to the phonon density of states.[15] We calculated the velocity autocorrelation function similarly to the dynamical structure factor by using the velocity data of every tenth simulation step of runs with a total length of 40 000 steps.

III. RESULTS

A. Phase diagram

On heating we observe a structural phase transition of the system in our simulations. Previous studies[2] showed that the bcc structure transforms to a close-packed structure with stacking faults. An analysis of the orientational relationships[3,24] revealed that during the transformation $(110)_{\mathrm{bcc}}$ planes transform into $(111)_{\mathrm{fcc}}$ planes leaving unrotated one $[001]_{\mathrm{bcc}}$ direction parallel to these planes. After the transformation this becomes the $[1\bar{1}0]_{\mathrm{fcc}}$ direction of the austenite phase. This is an example of a Nishiyama-Wassermann orientational relationship,[25] apart from the fact that the $(110)_{\mathrm{bcc}}$ planes are slightly rotated around $[001]_{\mathrm{bcc}}$.

The behavior of the potential energy of a $\mathrm{Fe}_{80}\mathrm{Ni}_{20}$ system over a complete temperature cycle in our simulations is shown in Fig. 1. During the structural phase transition taking place at 700 K the potential energy of the system goes down by approximately 0.2 mRy. This shows that the structural change is not an equilibrium phase transition but is strongly overheated. The other possibility that we were simply annealing to a more stable phase is clearly excluded by the behavior of the potential energy at low temperatures in Fig. 1. Nevertheless, the drop of the potential energy during the phase transition is remarkable, since it reflects the fact that the specific heat C_p of the high-temperature phase is lower than the specific heat of the low-temperature bcc phase which can also be seen from Fig. 1. This means that the entropy of the bcc phase is growing faster with temperature than the entropy of the close-packed phase. Therefore, in order to explain the occurrence of the phase transition, it must be concluded that in the limit $T\rightarrow 0$, where the entropy of a classical (harmonic) system goes to minus infinity, a finite difference between the entropies of both phases remains, which tends to favor the close-packed phase. This would mean that the phonon density of states at low frequencies is higher in the close-packed structure than in the bcc phase. If this is true, the correct quantum-mechanical treatment of the phonons would lead to a higher specific heat of the close-packed phase phase at low temperatures. It should be noted that in pure iron at the α-γ transition the specific

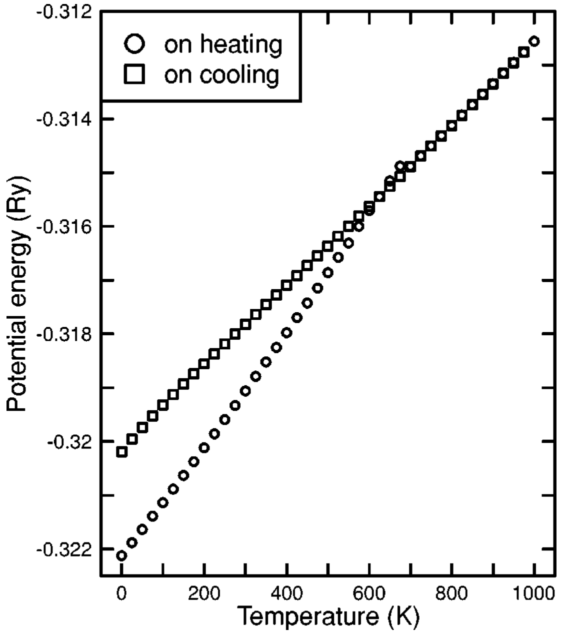

FIG. 1. Potential energy of $Fe_{80}Ni_{20}$ in our simulation during one complete temperature cycle starting at 0 K.

heat of the bcc phase is also considerably higher, which gives rise to the γ-δ transition at higher temperatures. The fact that it is very difficult to obtain the austenite-martensite transition in simulations with the potentials used in this work without the inclusion of an unphysically high number of vacancies has been discussed elsewhere.[3] Normally we find the same behavior as in Fig. 1, where the system stays in the close-packed phase down to the lowest temperatures.

In Fig. 2 the transition temperatures of the austenite transition observed in our molecular-dynamics simulations are compared with experimental results taken from Ref. 1. For Ni concentrations $x > 34\%$ the austenite transition cannot be observed experimentally since there is no martensite transition at these concentrations. However, it is possible to start simulations with a low-temperature bcc structure. Therefore, on the right side of Fig. 2 only results of simulations are shown. Another difference between simulation and experiment is given by the fact that experimentally there is not one definite transition temperature but an interval given by the austenite start and austenite final temperatures A_s and A_f. When the temperature increases from A_s to A_f an increasing fraction of the sample is transformed from martensite to austenite. In contrast to this in the simulations the system transforms rapidly at one temperature. This is a result of the small system sizes feasible in simulations together with long-range elastic interactions which prohibit phase coexistence on this length scale. Within these restrictions Fig. 2 shows a good agreement between simulation and experiment. Additional simulations[24] have demonstrated that the actual transition temperature in the simulation depends not only on the Fe concentration but also on the particular configuration of the atoms and the simulation time. The latter is a result of the fact that we deal with an overheated transition of first order.[2] Due to these uncertainties deviations from the calculated transition temperatures shown in Fig. 2 can occur which can be as large as 100 K.

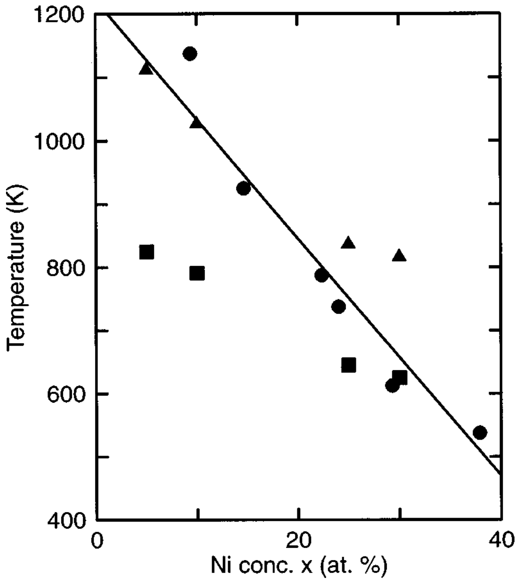

FIG. 2. Martensite-austenite transition temperatures of $Fe_{1-x}Ni_x$. Circles represent results of our molecular-dynamics simulations. The line results from a linear fit to these data. Squares and triangles represent measured transition temperatures (Ref. 1) A_s and A_f, respectively.

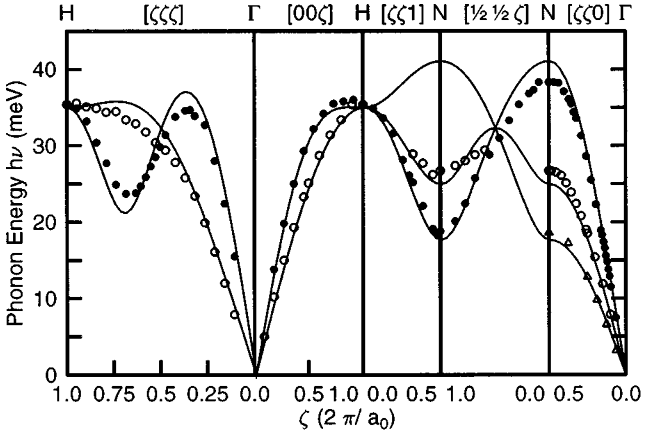

FIG. 3. Phonon-dispersion curves of bcc iron at $T = 0$ K. The solid lines are from calculations incorporating the EAM potential, and symbols are experimental data points (Refs. 13 and 27).

B. Phonon-dispersion curves of the metals

In a recent work[26] it has been pointed out by Simonelli *et al.* that EAM potentials often fail to reproduce the experimental phonon-dispersion relations. Therefore, we compare in Figs. 3 and 4 the phonon spectra of pure Fe and Ni, resulting from our EAM potentials, with experimental data obtained at room temperature. These data were obtained by diagonalization of the dynamical matrix without simulations. It can be seen that our model gives a good overall description of the vibrational properties of the metals. In order to clarify the effect of alloying on the phonon-dispersion relations of the metals we show in Fig. 5 the spectra of bcc Fe and Ni at the lattice constant $a_0 = 5.437$ a.u. This is the lattice constant

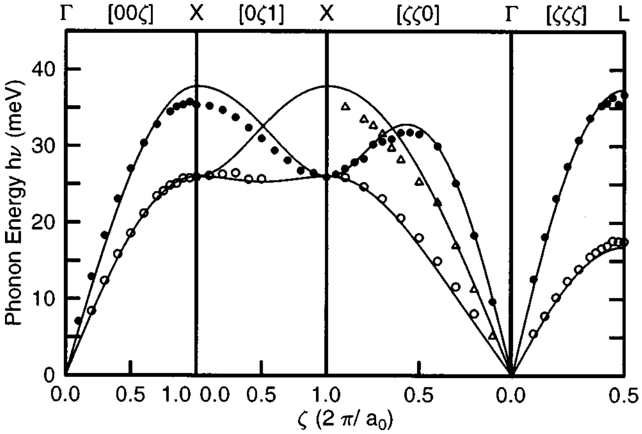

FIG. 4. Phonon-dispersion curves of fcc nickel at $T = 0$ K. The solid lines are from calculations incorporating the EAM-potential, and symbols are experimental data points (Ref. 14).

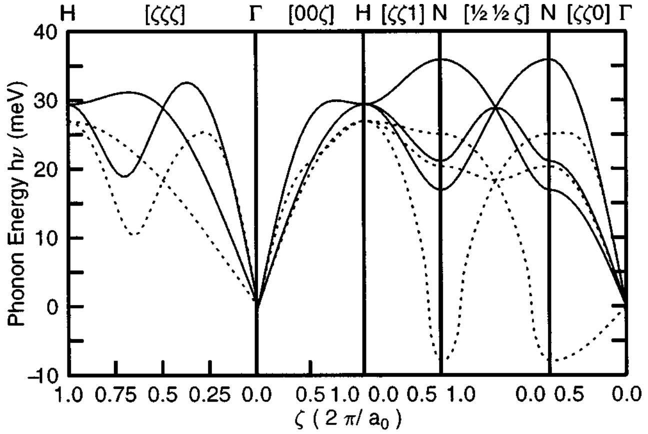

FIG. 5. Phonon-dispersion curves of Fe (solid line) and Ni (dotted line) in the bcc structure at $T = 0$ K calculated from the potentials, using a lattice constant $a_0 = 5.437$ a.u. Negative energies mean negative squares of frequencies.

we obtained for $Fe_{80}Ni_{20}$ at $T = 300$ K in our simulations. While the Fe spectrum shown in Fig. 5 differs only slightly from that in Fig. 3, due to the larger lattice constant, it can be seen from Fig. 5 that Ni is not stable in the bcc structure. Negative squares of frequencies occur around the N point and along the [110] direction. A similar instability has been found in electronic structure calculations of Ni which reveal a negative elastic constant C' (Ref. 28).

C. Phonon-dispersion curves of the alloy

From the molecular-dynamics simulations we obtained the phonon dispersion of $Fe_{80}Ni_{20}$ at $T = 300$ K along five high-symmetry directions. The results are presented in Fig. 6. These data were obtained by evaluation of the maxima of the peaks in the velocity autocorrelation function $g_{\alpha\alpha}(\mathbf{q},\omega)$. Very striking are the small energies of the [110]-TA_1 phonons (polarization along $[1\bar{1}0]$) and the crossing of longitudinal and transversal modes near the H point along the [100] direction. It can also be seen that the energies of the longitudinal mode around the N point of the Brillouin zone and around the H point are unusually high. The scattering of the data in regions of high phonon energies is an effect of damping and finite simulation time. Evaluation of the phonon frequencies from the position of the peaks of the dynamical structure factor gave essentially the same results. Only at phonon energies as high as 40 meV the latter method gives somewhat lower energies due to the shift of the peak maxima which is caused by the damping.

A comparison of the spectra of the pure metals in Figs. 3, 4, and 5 and the alloy (Fig. 6) shows that the spectrum of the alloy is closest to that of iron at its equilibrium lattice constant. The frequencies of the alloy are even higher than those of the metal, except for the low lying [110]-TA_1 branch. In contrast to this the spectrum of pure Fe at the lattice constant of the alloy in Fig. 5 shows significantly lower phonon energies. The influence of Ni is largest near the N point and along the [110] direction, i.e., in those regions, where Fig. 5 exhibits instabilities in the bcc structure of Ni. According to Fig. 5 the crossing of the modes along [100] in the alloy can also be attributed to the addition of Ni.

It is known that [110]-TA_1 phonons play an important role in bcc-fcc structural transitions.[25] In NiAl it is also known that the [110]-TA_1 branch of the bcc structure exhib-

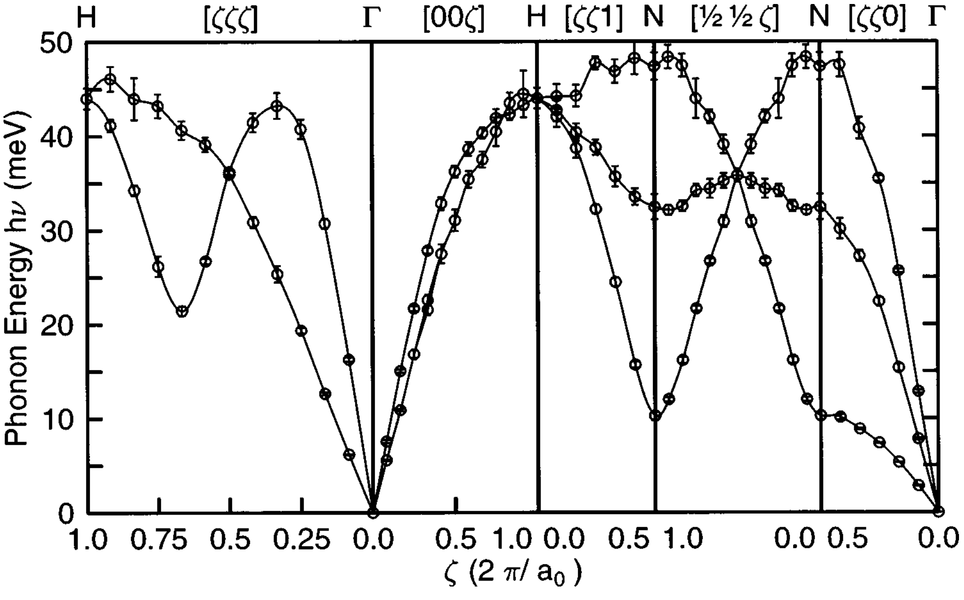

FIG. 6. Phonon-dispersion curves of $Fe_{80}Ni_{20}$ at $T = 300$ K determined from molecular-dynamics simulations. Data points and error bars represent averages and standard deviations of the results of the evaluation of $g_\alpha(\mathbf{q},\omega)$ in crystallographically equivalent directions. Lines are drawn as a guide to the eyes.

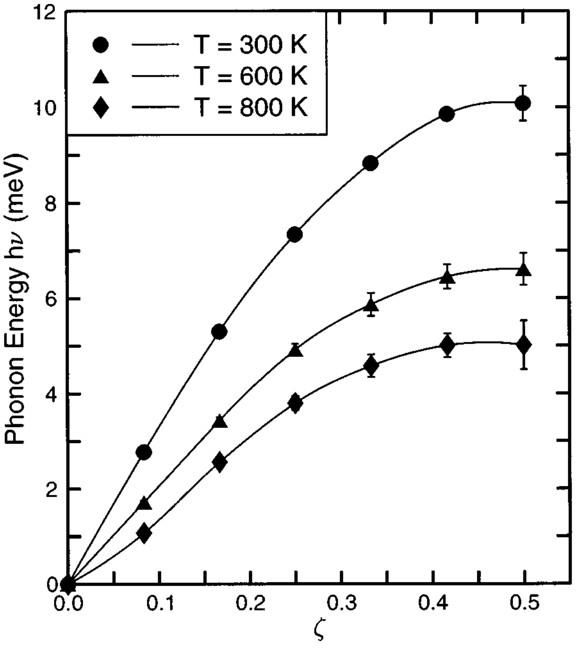

FIG. 7. Phonon dispersion of the $[110]$-TA_1 branch of $Fe_{80}Ni_{20}$ determined from molecular-dynamics simulations at different temperatures.

its temperature-dependent anomalies above the martensitic transformation.[4] Therefore, we have calculated the phonon-dispersion curves of $Fe_{80}Ni_{20}$ along this direction at different temperatures by evaluation of the positions of the peaks of the dynamical structure factor. While the longitudinal and transversal TA_2 mode exhibit only slight changes with temperature (less than 10% up to 300 K), the energies of the TA_1 mode exhibit a strong temperature dependence. This can be seen in Fig. 7, where the dispersion relations of the $[110]$-TA_1 phonon branch at different temperatures are shown. Between 300 and 800 K the phonon energies are reduced by about 50% along the whole branch. In the limit $\mathbf{q}\rightarrow\mathbf{0}$ this corresponds to a reduction of the elastic constant C' which determines the energy of one of the shears necessary for the bcc-fcc transition.[25]

Regarding the fact that the particular configuration used for the calculation of the phonon-dispersion curves exhibits the austenite transition well below 800 K, it is unlikely from Fig. 7 that $Fe_{80}Ni_{20}$ has a soft mode in the $[110]$-TA_1 branch at the transition temperature. This is illustrated more clearly in Fig. 8. Here the temperature dependence of the energies of the phonons with the lowest $\mathbf{q}$ vector accessible in our simulations is shown. One can clearly see a linear temperature dependence up to and beyond the transition temperature. Extrapolation of the fit in Fig. 8 shows that the energy of this mode would go to zero around $T=1120$ K. Therefore, it can be stated that the phonon anomalies observed in our simulations give no sign of a soft-mode transition. This is consistent with experimental observations in other systems (e.g., NiAl, Li) exhibiting martensitic transformations from a bcc austenite to a close-packed martensite.[4,5] Nevertheless, it has to be kept in mind that we have not directly probed the elastic behavior of the system right at the zone center.

The last question addressed in this paper concerns the occurrence of lifetime effects accompanying the frequency shift of the TA_1 mode. It has already been discussed that damping and lifetime effects can lead to a shift of the peaks in the dynamical structure factor. Similar effects have also been observed experimentally in the bcc to hcp transition of the elements Ti, Zr, and Hf.[29–31] Therefore, we have fitted the dynamical structure factor $S(\mathbf{q},\omega)$ to a function of the type of Eq. (6). Results of the oscillator energies $\hbar\omega_0$ and the friction coefficients Γ are given in Table V for some $\mathbf{q}$ vectors referring to different polarization directions and at the temperatures $T=300$ and 700 K. This table shows that there are strong effects in the friction constant Γ in all parts of the

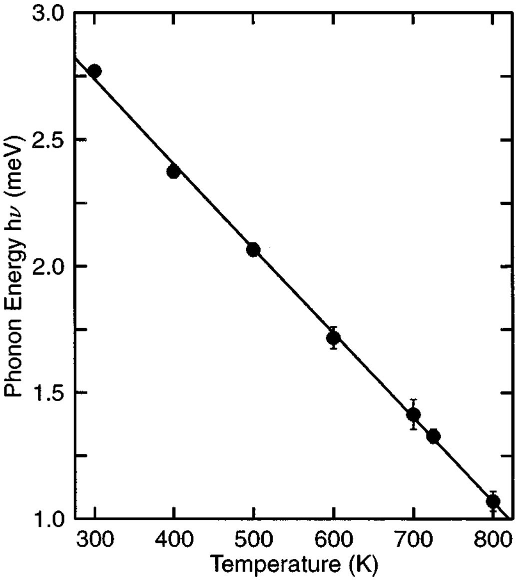

FIG. 8. Temperature dependence of the energy of the phonon with wave vector $\mathbf{q}=\frac{1}{12}[110]$ and polarization along $[\bar{1}10]$. The line results from a linear fit to the data points.

TABLE V. Results of fits of the dynamical structure factor $S(\mathbf{q},\omega)$ to a damped harmonic oscillator model [Eq. (6)]. Phonon energies $\hbar\omega_0$ and friction constants Γ are given in meV. In order to distinguish different polarization directions $S(\mathbf{q},\omega)$ has been evaluated at $\mathbf{q}=(2\pi/a_0)[(n/12)\,\mathbf{Q}+\mathbf{G}]$, where $\mathbf{G}$ is the wave vector of a Bragg peak along the corresponding polarization direction.

				$T=300$ K		$T=700$ K	
Q	Pol.	**G**	n	$\hbar\omega_0$	Γ	$\hbar\omega_0$	Γ
[100]	LA	**0**	1	7.528	0.900	7.140	1.390
			4	28.135	4.777	25.948	7.449
			12	44.580	15.772	42.777	25.611
	TA	[100]	1	5.482	0.964	5.279	1.145
			4	22.173	4.518	21.335	9.945
[110]	LA	**0**	1	12.979	2.025	12.336	4.141
			6	48.831	16.570	45.352	20.407
	TA_2	[002]	1	7.738	1.251	7.445	2.149
			6	31.508	9.667	30.765	16.259
	TA_1	$[\bar{1}10]$	1	2.797	0.557	1.549	0.739
			6	10.168	2.100	6.443	3.068
[111]	LA	**0**	1	16.494	2.675	15.701	4.204
			4	43.368	12.130	40.530	15.778
	TA	$[\bar{1}10]$	1	6.149	1.080	5.369	1.302
			4	25.034	5.280	23.541	10.534

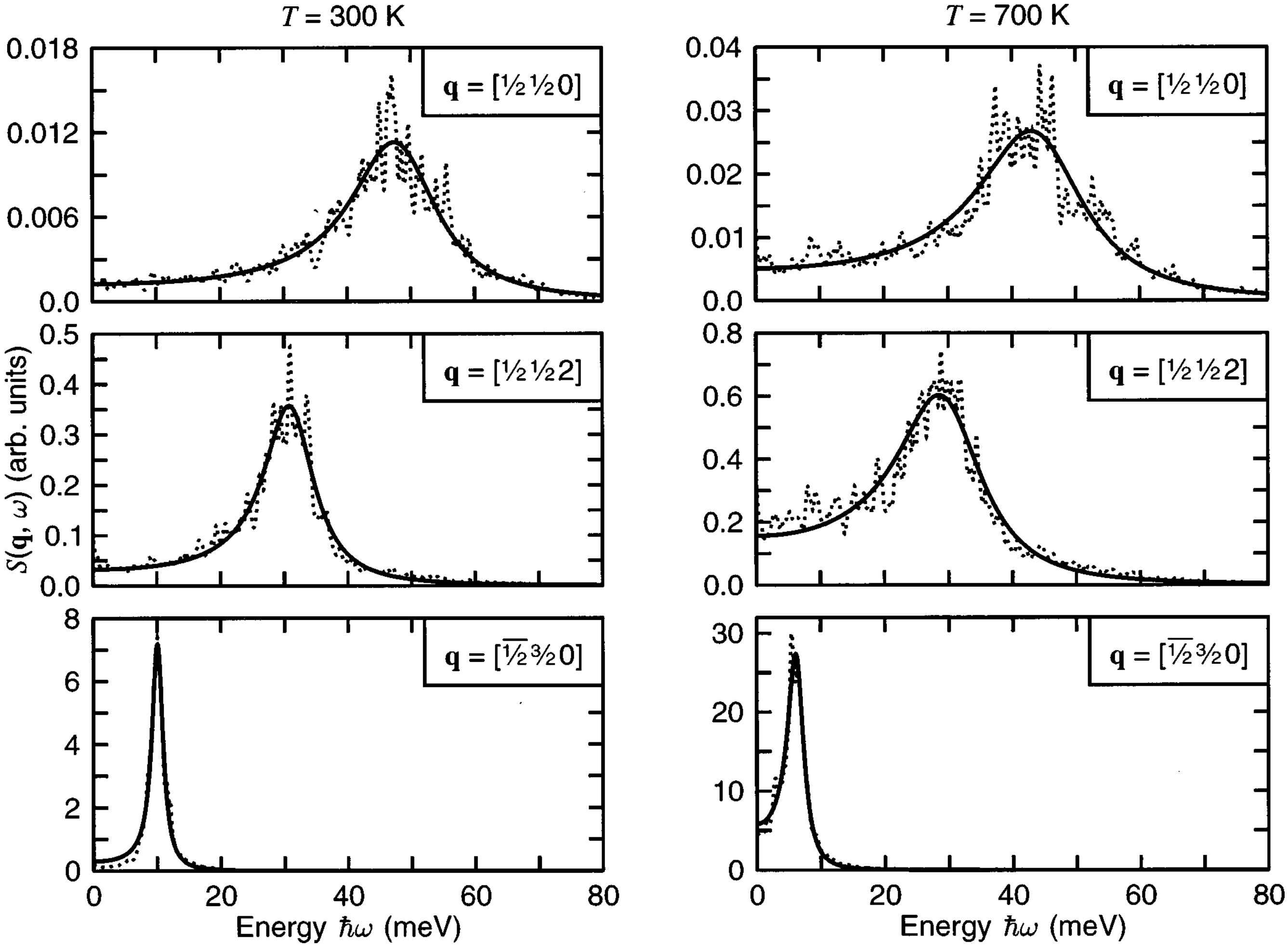

FIG. 9. Dynamical structure factor $S(\mathbf{q},\omega)$ at $T=300$ and 700 K. Dotted lines show the results of molecular-dynamics simulations broadened by a linewidth of 0.5 meV, solid lines represent fits of these data to a damped harmonic oscillator model [Eq. (6)].

Brillouin zone and all polarization modes. However, these effects do not account for the shift of the peak maxima of the TA_1 modes along the [110] direction. This is the only mode showing a considerable effect of the frequency ω_0. This is further illustrated by Fig. 9 which shows the dynamical structure factor and the corresponding fit functions of all polarization modes at the N point. The strong oscillations of the simulation results in Fig. 9 are a consequence of the small signal amplitude and the finite simulation time. It should also be noted that the fit results given for ω_0 in Table V agree very well with the results in Fig. 6 obtained from the position of the peaks of the velocity autocorrelation function.

IV. SUMMARY AND CONCLUSIONS

Our molecular-dynamics simulations of the austenite transition in $Fe_{1-x}Ni_x$ reveal that the model developed for the description of these alloys,[2] reproduces the experimentally observed martensite-austenite transition very well. On the other hand, it is has been discussed in Ref. 3 that the corresponding austenite-martensite transition cannot be found in simulations using this model without the inclusion of high defect densities. This is due to the fact that the potential includes no explicit magnetic terms. Magnetism enters the model only in the fit to the experimental data. This might lead to a bad description of the energy difference between the fcc phase and the bcc phase at low temperatures and thereby suppress the austenite-martensite transition. On the other hand, the good agreement between the transition temperatures with experiment shows that entropy contributions of lattice vibrations play an important role in the martensitic transformation in $Fe_{1-x}Ni_x$. As has been pointed out, the observed behavior of the specific heat in our simulations is also similar to the behavior of pure iron. Since in pure iron this gives rise to the γ-δ transition the same might be true for our model system, though, we have not succeeded in observing such a transition so far.

The good agreement between experimental and calculated phonon-dispersion relations is a consequence of the fact that we have used selected phonon frequencies during the construction of the potentials. This is in accordance with Ref. 26, where it is stated that it should be possible to obtain a reasonably good description of the vibrational and elastic properties of Fe with EAM potentials. Ni should even work better. Nevertheless, the good agreement between experiment and model in the case of the pure metals does not necessarily lead to a good description of the alloy, since the properties of the alloy did not enter into the construction of the potentials.

We have used two distinct methods for the evaluation of the phonon spectra. While the velocity autocorrelation function $g_{\alpha\alpha}(\mathbf{q},\omega)$ does not show anomalous Brillouin-zone behavior the dynamical structure $S(\mathbf{q},\omega)$ factor can be compared directly with data from neutron-scattering experiments. Differences between the two methods occur at high phonon energies, where the peaks of the dynamical structure factor are shifted by damping effects. Fitting of $S(\mathbf{q},\omega)$ to a damped harmonic oscillator model brings both methods in a line and gives additional information about phonon lifetimes.

The phonon-dispersion curves of $Fe_{80}Ni_{20}$ derived from molecular-dynamics simulations are dominated to a high degree by the spectrum of pure Fe at its equilibrium lattice constant. The low lying $[110]$-TA_1 mode can be attributed to the instabilities in the spectrum of bcc-Ni along this direction. Similarly the crossing of the frequencies of longitudinal and transversal modes near the H point is a direct consequence of the vibrational properties of Ni with bcc structure. The strong temperature dependence of the $[110]$-TA_1 mode in our simulations is similar to that observed in bcc austenite systems. This leads to the conclusion that in $Fe_{1-x}Ni_x$ the bcc structure becomes unstable by a similar mechanism as in the nonferrous systems. This is consistent with the very large hysteresis of the transition temperatures in $Fe_{1-x}Ni_x$ and the fact that fcc Fe remains metastable even at very low temperatures. Fits of the dynamical structure factor to a damped harmonic oscillator model revealed that the temperature driven shifts of the phonon frequencies cannot be explained by means of shorter phonon lifetimes, though damping effects can be seen all over the Brillouin zone.

According to our knowledge, up to now there are no experimental data available of the phonon-dispersion relations of $Fe_{80}Ni_{20}$. In pure bcc Fe a similar, though less pronounced, softening of the $[110]$-TA_1 branch has been observed.[32] It is possible that the EAM potentials overestimate the temperature dependence of the phonon spectrum due to the missing treatment of magnetism which in turn might lead to similar effects as described in Ref. 33. However, it is very likely from Fig. 6 that the temperature-driven reduction of the $[110]$-TA_1 branch is enhanced by the addition of Ni due to the instability of bcc Ni shown in Fig. 5. It would be very interesting to see if these theoretical predictions can be confirmed experimentally.

ACKNOWLEDGMENTS

R.M. wishes to thank M. Acet, H. C. Herper, and S. Lübeck for many helpful discussions. We gratefully acknowledge the Höchstleistungsrechenzentrum Jülich, Germany, for giving us CPU time on its Intel Paragon and Cray T3E parallel computers. This work has been supported by the Deutsche Forschungsgemeinschaft (SFB 166).

---

*Electronic address: ralf@thp.Uni-Duisburg.DE

†Electronic address: entel@thp.Uni-Duisburg.DE

[1] M. Acet, T. Schneider, and E. F. Wassermann, J. Phys. IV **C2**, 105 (1995).

[2] R. Meyer and P. Entel, J. Phys. IV **C2**, 123 (1995).

[3] R. Meyer, K. Kadau, and P. Entel, in *Properties of Complex Inorganic Solids*, edited by A. Gonis, A. Meike, and P. E. A. Turchi (Plenum, New York, 1997).

[4] S. M. Shapiro, B. X. Yang, Y. Noda, L. E. Tanner, and D. Schryvers, Phys. Rev. B **44**, 9301 (1991).

[5] R. J. Gooding and J. A. Krumhansl, Phys. Rev. B **38**, 1695 (1988).

[6] M. S. Daw and M. I. Baskes, Phys. Rev. Lett. **50**, 1285 (1983); Phys. Rev. B **29**, 6443 (1984).

[7] S. M. Foiles, M. I. Baskes, and M. S. Daw, Phys. Rev. B **33**, 7983 (1986).

[8] E. Clementi and C. Roetti, At. Data Nucl. Data Tables **14**, 167 (1974). We use the double -ζ functions on p. 433.

[9] W. Bendick and W. Pepperhoff, Acta Metall. **30**, 679 (1982).

[10] L. Kaufman and H. Bernstein, *Computer Calculations of Phase Diagrams* (Academic, New York, 1970), p. 185.

[11] J. A. Rayne and B. S. Chandrasekhar, Phys. Rev. **122**, 1714 (1961).

[12] G. A. Alers, J. R. Neighbours, and H. Sato, J. Phys. Chem. Solids **13**, 40 (1960).

[13] V. J. Minkiewicz, G. Shirane, and R. Nathans, Phys. Rev. **162**, 528 (1967).

[14] R. J. Birgenau, J. Cordes, G. Dolling, and A. D. B. Woods, Phys. Rev. **136**, A1359 (1964).

[15] M. P. Allen and D. J. Tildesley, *Computer Simulations of Liquids* (Clarendon, Oxford, 1987).

[16] S. Nosé, Mol. Phys. **52**, 255 (1984).

[17] W. G. Hoover, Phys. Rev. A **31**, 1695 (1985).

[18] M. Parrinello and A. Rahman, Phys. Rev. Lett. **45**, 1196 (1980); J. Appl. Phys. **52**, 7182 (1981).

[19] N. W. Ashcroft and N. D. Mermin, *Solid State Physics* (Holt, Rinehart, and Winston, New York, 1976), p. 792.

[20] S. W. Lovesey, *Theory of Neutron Scattering from Condensed Matter* (Clarendon, Oxford, 1984), Vol. 1, p. 301.

[21] B. L. Zhang, C. Z. Wang, K. M. Ho, D. Turner, and Y. Y. Ye, Phys. Rev. Lett. **74**, 1375 (1995).

[22] H. R. Schober and W. Petry, in *Structure of Solids*, edited by V. Gerold, Materials Science and Technology, Vol. 1 (VCH, Weinheim, 1993), p. 346.

[23] C. Z. Wang, A. Fasolino, and E. Tosatti, Phys. Rev. B **37**, 2116 (1988).

[24] K. Kadau (unpublished).

[25] W. Petry, J. Phys. IV **C2**, 15 (1995).

[26] G. Simonelli, R. Pasianot, and E. J. Savino, Phys. Rev. B **55**, 5570 (1997).

[27] B. N. Brockhouse, H. E. Abou-Helal, and E. D. Hallman, Solid State Commun. **5**, 211 (1967).

[28] E. Hoffmann (unpublished).

[29] W. Petry, A. Heiming, J. Trampenau, M. Alba, C. Herzig, H. R. Schober, and G. Vogl, Phys. Rev. B **43**, 10 933 (1991).

[30] A. Heiming, W. Petry, J. Trampenau, M. Alba, C. Herzig, H. R. Schober, and G. Vogl, Phys. Rev. B **43**, 10 948 (1991).

[31] J. Trampenau, A. Heiming, W. Petry, M. Alba, C. Herzig, W. Miekeley, and H. R. Schober, Phys. Rev. B **43**, 10 963 (1991).

[32] J. Neuhaus, K. Nicolaus, W. Petry, B. Hennion, and A. Krimmel, Physica B **234-236**, 897 (1997).

[33] R. J. Wolf, K. Mansour, M. W. Lee, and J. R. Ray, Phys. Rev. B **46**, 8027 (1992).